Vacuum 209 (2023) 111808

Contents lists available at ScienceDirect

Vacuum

journal homepage: www.elsevier.com/locate/vacuum

Strain effect on the phonon transport properties of hydrogenated 2D GaN

Guoqing Sun, Yanhua Cheng, Jinlong Ma, Dongwei Xu *, Xiaobing Luo

State Key Laboratory of Coal Combustion, School of Energy and Power Engineering, Huazhong University of Science and Technology, Wuhan, 430074, China

ARTICLE INFO

Keywords:
Hydrogenated GaN
Thermal conductivity
Anharmonicity
Electronic structure

ABSTRACT

Surface hydrogenation on 2D GaN has received extensive attention since surface passivation broadens its application in electronic devices. Strain is inevitably introduced in the process of 2D material synthesis, and its effects on thermal transport need to be discussed. In this work, we performed a detailed study on the strain-dependent thermal transport properties of hydrogenated monolayer GaN (H-GaN). With the increasing of strain, the thermal conductivity of H-GaN rises first and then descends, showing a volcanic shape. Detailed analyses show that the primary factor affecting the trend origins from the change of phonon lifetime. Fundamental understanding of the lifetime trend is achieved by electronic structures. It is found that due to the competition between the polarity and strength of Ga-N bond, atom vibration anharmonicity first drops and then enhances with the increasing of strain. Moreover, mean free path shows that strain combined nanostructure engineering could regulate the thermal transport properties effectively due to size effect.

1. Introduction

Gallium nitride (GaN), as a third generation semiconductor material with wide band gap (3.4 eV) [1] and high thermal conductivity (227 Wm^{-1} K^{-1}) [2], has been widely used in optoelectronic applications like light emitting diodes [3] and laser diodes [4,5]. With the trend toward miniaturization of photoelectric devices, two dimensional (2D) monolayer GaN has also attracted a lot of attention. However, the indirect electronic band gap (2.184 eV) [6] greatly limits its application in photoelectric devices. Fortunately, the unsaturated bond of pristine monolayer GaN provides a way to modulate the electronic structure by surface modification. The bandgap of hydrogenated GaN (H-GaN) tunes from indirect to direct, and the binding energy is also reduced [7,8], making buckling hydrogen adsorbed structure the most stable form of 2D monolayer GaN [9–11]. Further studies have shown H-GaN's tunable electronic and magnetic properties via strain and vacancy defects, and the investigations on optical property also show its promising application in nonlinear optics [11–13].

In practice, substrates are needed during the synthesis of 2D materials, to provide a platform for crystal growth. However, lattice mismatches and differences in the coefficient of thermal expansion between substrate and target product lead to strain [14,15]. For example, uniform lattice increment of 4.17% is found when 2D GaN single crystal is synthesized on liquid metals [16], and twisted bilayer graphene holds strain value as high as 15% when it is grown on the Ni surface by chemical vapor deposition [17]. 2D semiconductors can endure strain higher than 10%, which is much larger than bulk materials (0.5%–1.5%) [18]. It has been proved that strain formed by lattice mismatch modifies the electronic structure [19] and optical properties [10,20]. Inspired by the interesting properties caused by intrinsic strain in 2D materials, great efforts have been devoted to artificially and accurately introduce the strain [21]. Many methods have been developed, such as pre-stretched substrates [22], directly stretching [23], alloying and doping [24,25]. Those method have been applied to 2D materials. For example, uniaxial strain > 10% of graphene was obtained by directly stretching [23], and 10% tensile strain could be introduced into 2D BP using pre-stretched substrates [22].

An important factor affecting the performance of photoelectric devices during its work is the thermal transport property. Low thermal conductivity will cause heat accumulation and may damage the device. Given the inevitability of strain, it is necessary to study its influence on thermal transport. For the most common 2D planar hexagonal structures, Qin et al. applied tensile strain in hexagonal planar structure [26], and the thermal conductivities of GaN and AlN increase first and then decrease (up-then-down) with the increase of strain, which is because of the unbonded lone-pair electrons. For monolayer 2D materials with slight buckling (mainly IVA/VA materials), thermal conductivities of AsP [27] and silicene [28] increase first and then decrease under large strain, while antimonene [29] and germanene [30] increase over the entire tensile strain range. In that structure, the increased thermal conductivity under small strain results from the increase of out-of-plane vibration (ZA) mode's lifetime. More complex 2D structures had further been studied [31–34], and the complex bonding properties provide more diverse reasons for variations in thermal conductivity. For

* Corresponding author.
E-mail address: dwxu@hust.edu.cn (D. Xu).

https://doi.org/10.1016/j.vacuum.2023.111808
Received 10 October 2022; Received in revised form 2 January 2023; Accepted 2 January 2023
Available online 5 January 2023

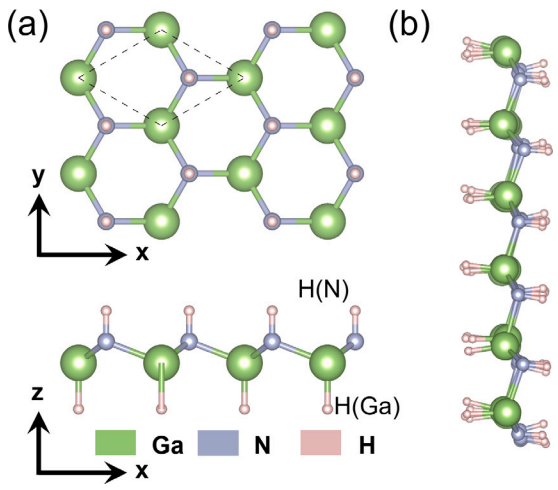

Fig. 1. (a) Structure of H-GaN, the dashed lines represent for the unit cell. (b) Structure of H-GaN at strain of 10% from AIMD simulation at 300 K after 2 ps.

2D penta-graphene, penta-SiC_2, and penta-SiN_2, the thermal conductivity show a monotonous decrease, nonmonotonic up-then-down, and jump at buckled-to-planar structure transition with increased tensile strain, respectively [35]. Although the thermal conductivities of some materials show similar trend, the underlying phonon properties are different. It can be seen that the regulating effects of strain on 2D materials greatly dependent on the material and the structure.

In this work, detailed thermal transport properties are studied from a combination of first-principles calculations and the linearized phonon Boltzmann equation. It is found that thermal conductivity of H-GaN shows an up-then-down trend with strain increases from 0% to 10%. Both the harmonic and anharmonic properties are discussed, and the electronic structures are further analyzed to gain a deeper insight.

2. Computational details

First-principle calculations are performed within generalized gradient approximation (GGA) exchange–correlation functional of Perdew–Burke–Ernzerhof (PBE) [36], as implemented in the VASP code [37,38]. And the projector-augmented-wave (PAW) potentials are used for Ga, N and H, where the *3d* electrons of Ga are classified as valence electrons. The unit cell of H-GaN is built with a 20 Å vacuum region to avoid spurious interactions. Different levels of biaxial tensile strain (ϵ) are imposed in increments of 2% by changing the lattice constant (l) from the unstrained value (l_0) as

$$\varepsilon = \frac{l - l_0}{l_0} \times 100\% \tag{1}$$

The structures are fully relaxed until the convergence criterion for force and energy become less than 10^{-6} eV Å^{-1} and 10^{-8} eV, respectively. A Gamma-centered 15 × 15 × 1 k-mesh is used to sample the Brillouin zone, and the energy cut-off for the plane wave basis is set to 600 eV during structure optimization.

Thermal transport properties are obtained by solving the phonon Boltzmann transport equation (BTE) using ShengBTE code [39]. In this framework, The lattice thermal conductivity tensor can be written as

$$k^{\alpha\beta} = \frac{1}{k_B T^2 8\pi^3} \sum_{\lambda} \int (f_0^2 + f_0)\hbar^2 \omega_{\lambda,q}^2 v_{\lambda,q}^{\alpha} v_{\lambda,q}^{\beta} \tau_{\lambda,q} dq \tag{2}$$

where ω and f_0 are phonon frequency and phonon distribution function, and ω is obtained by diagonalizing the dynamic matrix. λ and $\mathbf{q}$ are phonon branch and wave vector, respectively, and α and β are Cartesian directions. v and τ represent phonon group velocity and lifetime, which are usually decisive for thermal conductivity. Phonon lifetime can be determined by Matthiessen's rule *via* the following formula [40]

$$\tau_{\lambda}^{-1} = \tau_{\lambda,anh}^{-1} + \tau_{\lambda,iso}^{-1} + \tau_{\lambda,B}^{-1} \tag{3}$$

where τ_{λ} is total phonon lifetime. $\tau_{\lambda,anh}$, $\tau_{\lambda,iso}$ and $\tau_{\lambda,B}$ stand for phonon lifetime due to intrinsic phonon–phonon scattering, isotope scattering and phonon-boundary scattering, respectively. The scattering process is mostly contributed by anharmonic phonon–phonon scattering in an infinitely periodic system, and $\tau_{\lambda,anh}^{-1}$ is determined by Xie et al. [28]

$$\tau_{\lambda,anh}^{-1} = \frac{1}{N}\left(\sum_{\lambda'\lambda''}^{+} \Gamma_{\lambda\lambda'\lambda''}^{+} + \frac{1}{2}\sum_{\lambda'\lambda''}^{-} \Gamma_{\lambda\lambda'\lambda''}^{-}\right) \tag{4}$$

where N is the number of $\mathbf{q}$ points. $\Gamma_{\lambda\lambda'\lambda''}^{+}$ and $\Gamma_{\lambda\lambda'\lambda''}^{-}$ represent absorption ($\lambda + \lambda' \rightarrow \lambda''$) and emission ($\lambda \rightarrow \lambda' + \lambda''$) process [41].

Interatomic force constants (IFCs) required by solution of the BTE are obtained using the first-principles-driven lattice dynamics calculations. The phonon dispersion based on the second-order IFCs are calculated using the PHONOPY package [42] with a 6 × 6 × 1 supercell. To take the long-range electrostatic interactions into account, Born effective charges and dielectric constants are calculated using density functional perturbation theory (DFPT). Supercell of 5 × 5 × 1 (containing 100 atoms) is adopted to calculate the third-order IFCs using finite displacement method [43], and the Brillouin zone is sampled by a 1 × 1 × 1 grid. To get a convergent thermal conductivity, we consider the interactions up to 6th nearest neighbors, while the q-meshes of 80 × 80 × 1 is used. For a 2D material involved in thermal transport, all the heat flux has to pass through it, no matter how thick it is Wu et al. [44]. Thus, to achieve a fair comparison among different strain levels, the thickness of all 2D structures is defined to be 5.47 Å in this work, which is the buckling distance plus the sum of the van der Waals radii of outer-most atoms of H-GaN in the free-standing state. Using Voigt–Reuss–Hill model [45], Young's modulus is obtained. To verify the thermal stability of H-GaN under strain, the ab initio molecular dynamics (AIMD) simulation is performed using 5×5×1 supercell under the canonical (NVT) ensemble at 300 K for 2 ps, with time step of 1 fs.

3. Results and discussion

3.1. Structures and thermal conductivity

H-GaN has a graphene-like hexagonal structure as shown in Fig. 1(a). The pristine 2D GaN exhibits a perfect planar structure due to its dangling bonds [5]. Hydrogenation saturates the configuration, and the planar sp^2 hybridization changes to tetrahedrally coordinated sp^3-like orbitals, resulting in a buckled structure and the degenerated space symmetry (*P3m1*) of H-GaN. Phonon dispersion curves under different strain levels are shown in Fig. 2(a) and (b). The absence of imaginary modes in the Brillouin zone confirms the dynamically stability of H-GaN under tensile strain. The thermodynamic stability under strain of 10% is also verified by the stable structure during AIMD simulation shown in Fig. 1(b). Small fluctuation of temperature and energy shown in Fig. S2 further verifies its stability. From the phonon spectrum, the light H atoms mainly contribute to the high frequency, while acoustic modes are mainly contributed by Ga and N. The lack of reflection symmetry selection rule elevates the frequency of the ZO mode above the acoustic branches in H-GaN compared to that in pristine monolayer GaN [8]. The normalized thermal conductivity as a function of frequency shown in Fig. 2 (a) indicates that the thermal conductivity is mainly determined by the phonons under 7 THz. This is due to the Bose–Einstein distribution obeyed by phonon population, which allows phonons mainly occupy low frequency modes. With tensile strain increases from 0% to 10%, it is clearly seen that optical branches move downward with the increasing tensile strain, which is the result of reduced material stiffness (as revealed by Young's

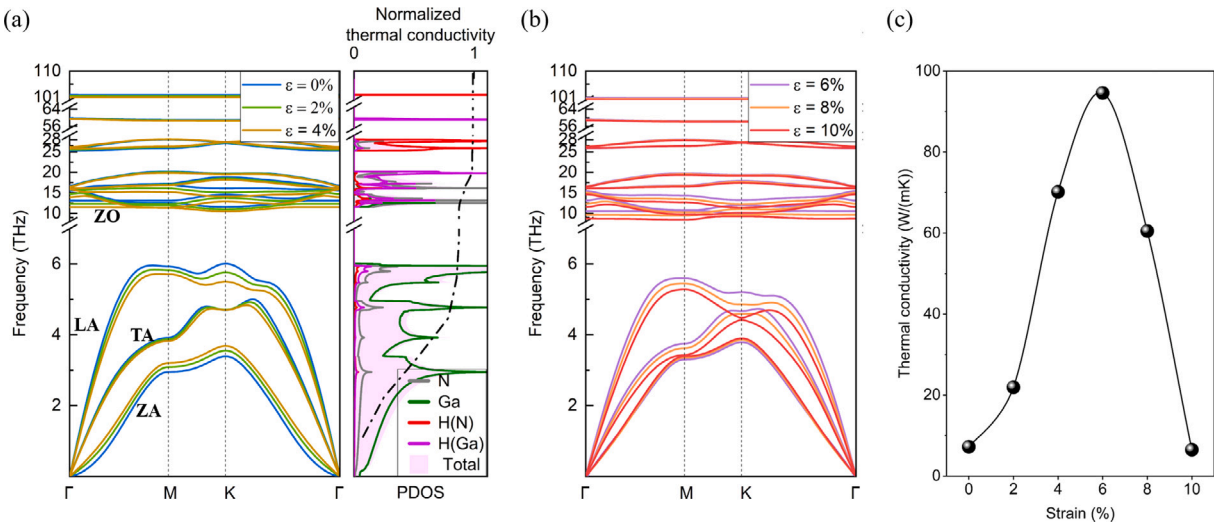

Fig. 2. Phonon dispersion curves of H-GaN at strain of 0%, 2%, 4% and (b) 6%, 8%, 10%. The right panel in (a) shows the phonon projected density of state, and the black dash line represents the normalized thermal conductivity as a function of frequency. (c) Thermal conductivity of H-GaN at 300 K under different strain levels.

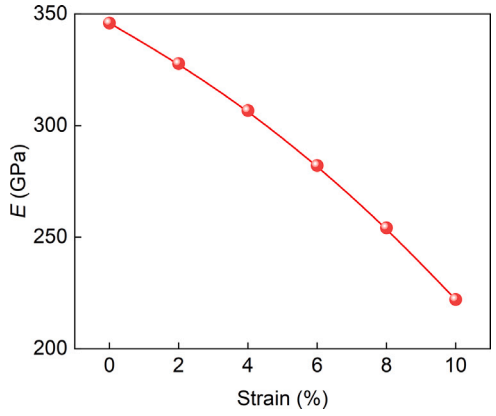

Fig. 3. Young's modulus of H-GaN under different strain levels.

modulus in Fig. 3). As for the acoustic branches, LA and TA are the in-plane longitudinal and transverse modes, while ZA is the out-of-plane bending mode in 2D materials. It can be seen from Fig. 2 that ZA curve shows quadratic dispersion near the Γ point in the case of zero strain, which can be explained by the elastic theory of a thin plate [46]. With the increasing of strain, ZA becomes linearized, while the slopes of LA and TA decrease.

The thermal conductivity at 300 K as a function of strain is depicted in Fig. 2(c). The calculated thermal conductivity of free-standing H-GaN are 7.24 W m^{-1} K^{-1}. H-GaN shows an up-and-down behavior with strain increasing from 0% to 10%. It increases to the maximum of 94.58 W m^{-1} K^{-1} at the strain of 6% and then decrease greatly to 6.51 W m^{-1} K^{-1} at 10%. The results show that thermal conductivity of H-GaN exhibits good tunability. To find the underlying reasons for the variation of thermal conductivity, Phonon harmonic and anharmonic properties under strain are further discussed below.

3.2. Harmonic properties

Phonon mode group velocities under different strain levels are calculated using second-order force constants and are plotted in Fig. 4. We have ignored the optical phonons in Fig. 4 since that optical modes have little effect on thermal conductivity, as discussed in Section 3.1. In general, the group velocity of H-GaN shows a decreasing trend with the increases of strain. Specifically, the maximum group velocity of TA and LA mode is reduced from 4.5 km s^{-1} to 3.5 km s^{-1} and 6.7 km s^{-1} to 5.4 km s^{-1} at 10% tensile strain, respectively. These results are consistent with the decreasing slope trends of TA and LA as shown in Fig. 2, which are caused by the weakened interatomic interaction induced by tensile strain. The weakened interatomic interaction could be revealed by the decrease of Young's modulus from 346 GPa to 184 GPa shown in Fig. 3. Different from the in-plane acoustic modes, the group velocities of ZA modes are close to zero near Γ point at the strain-free state. As the in-plane strain increases to 10%, the lattice becomes stiffer to out-of-plane bending vibration [47,48], resulting in the linearized ZA branches and increased phonon velocity (about 2.0 km s^{-1} at the strain of 10%). As can be seen from above, the mode group velocity is consistent with the change of mechanical properties of H-GaN caused by the in-plane strain. However, it is hard to give explanations for the up-then-down trend with the increase of strain. To this end, we further calculate the anharmonic properties.

3.3. Anharmonic properties

The phonon lifetime can be calculated using a three-phonon scattering rate from third-order anharmonic IFCs. The mode-level phonon lifetime is shown in Fig. 5, considering acoustic phonons are the dominant heat carriers in the heat transport in H-GaN, we only show the lifetime of for acoustic modes. As strain increases from 0% to 6%, all acoustic modes' lifetime increase, which coincides with the increased thermal conductivity from 7.24 W m^{-1} K^{-1} to 94.58 W m^{-1} K^{-1}. And the ZA mode's lifetime with the largest increase reaches 3 to 4 orders of magnitudes. However, as the strain increases further, the overall phonon lifetime shows a decline trend, which agrees well with the low thermal conductivity of H-GaN at the strain of 10%. As can be seen from above, the up-then-down trend of phonon lifetime agree well with the variation of thermal conductivity with strain.

Considering lattice vibration anharmonicity is the fundamental factor affecting phonon lifetime, and electronic structures determine the physical properties of crystal. We will explore how the lattice anharmonicity is driven by the bonding properties of H-GaN.

3.4. Insight from electronic structures

Lone-pair-electrons usually have non-negligible effects on the thermal transport properties [49–52], and it also exists and plays an important role in monolayer GaN [53]. In H-GaN, surface hydrogenation eliminates this effect by saturating the configuration. Moreover, considering H atom mainly contributes to the high frequency phonons,

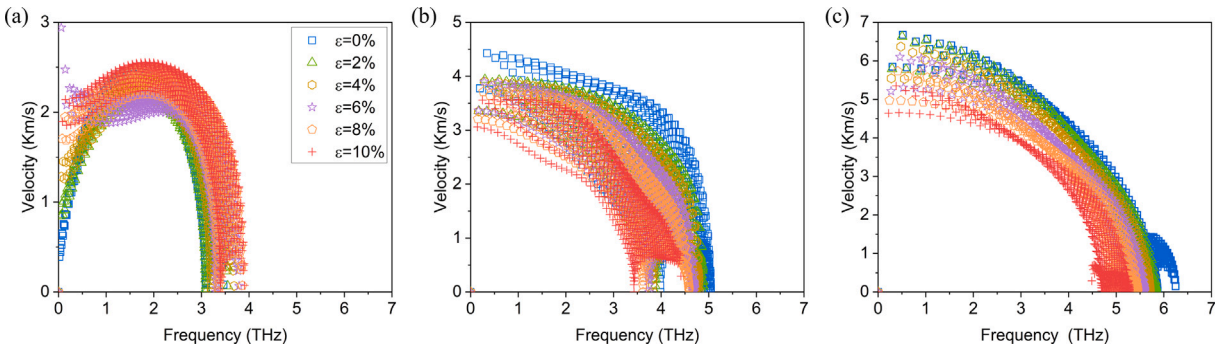

Fig. 4. The phonon mode group velocity ((a) ZA (b) TA (c) LA) of H-GaN under strain.

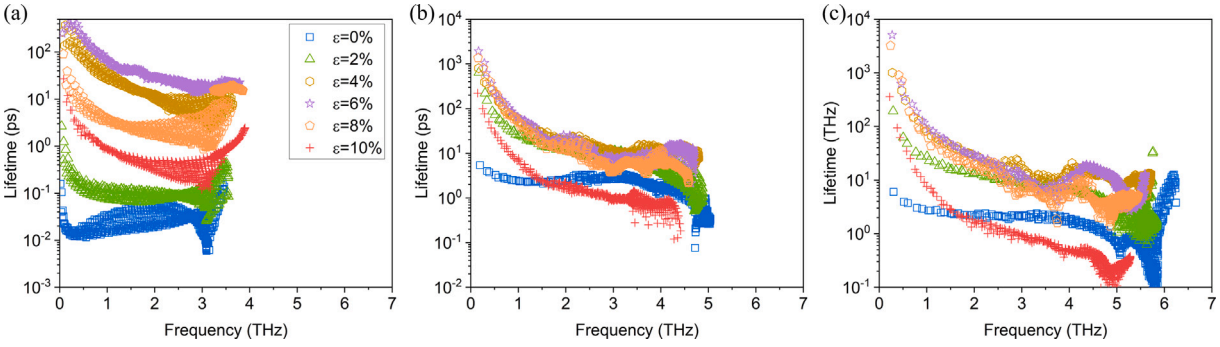

Fig. 5. The phonon mode lifetime ((a) ZA (b) TA (c) LA) of H-GaN under strain.

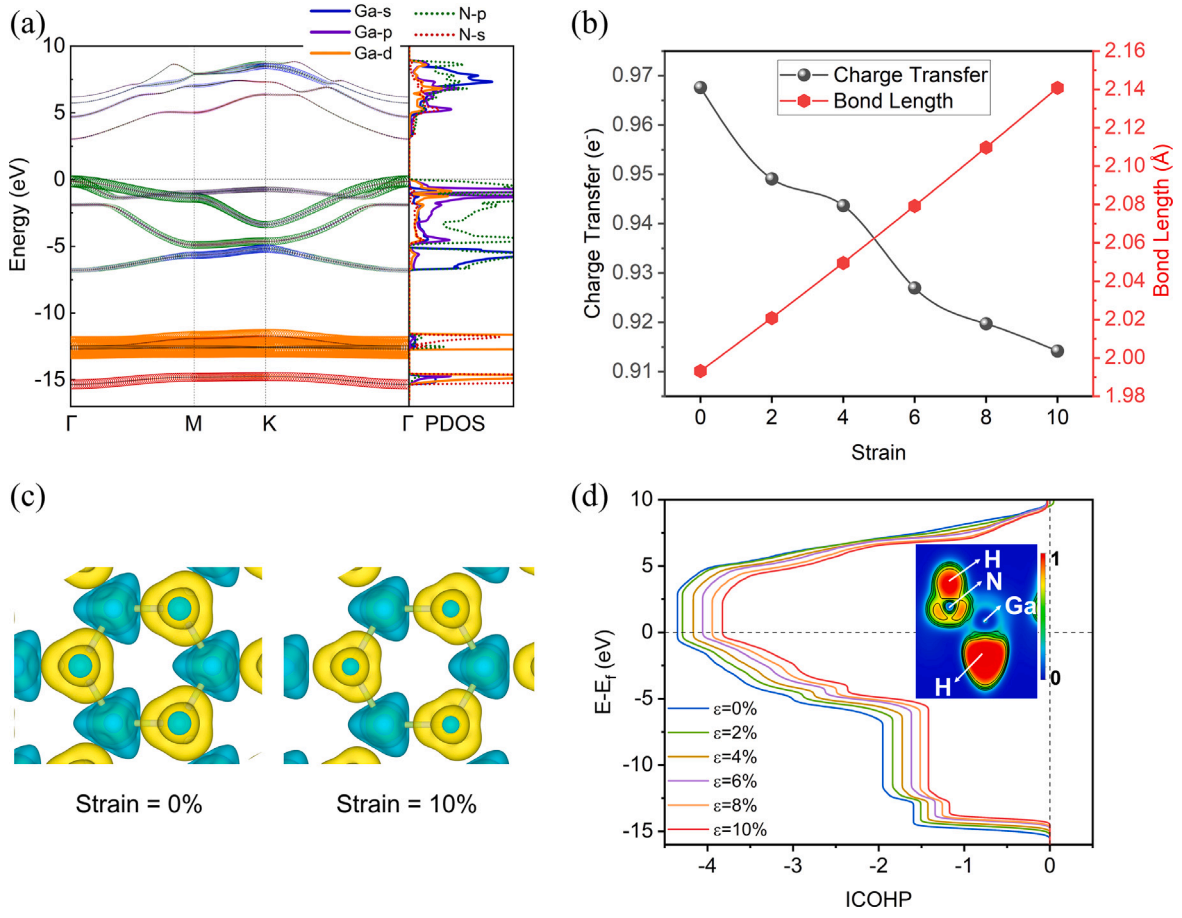

Fig. 6. (a) Band structure and projected density of state of H-GaN. (b) Charge transfer and bond length between Ga and N under different strain levels. (c) Deformation charge density of H-GaN in 3D view at the strain of 0% and 10%, the isosurface is set to be 0.009 eÅ^{-3}. (d) ICOHP of Ga-N interaction in H-GaN under strain. The energy axis, shifted such that the Fermi level lies at 0 eV. The inset shows the ELF.

Table 1
The rMFP of H-GaN under different strain level.

Strain (%)	0	2	4	6	8	10
rMFP (nm)	11.0	63.4	232.7	813.9	552.5	46.5

which have very little effects on the thermal conductivity, we will focus mainly on Ga-N pair. The ELF (electronic location function) is shown in Fig. 6(d). ELF measures the extent of spatial localization of the reference electron physically, where 0 means no electron, 0.5 corresponding to the electron gas, and 1 corresponding to perfect localization. The localized electronic state between *N* and Ga atoms clearly reveals the covalent Ga-N bond. From the projected density of states shown in Fig. 6(a), bonding of H-GaN is not a simple sp^3 bonding scheme by forming four separate subbands below VBM (valence band maximum) like bulk GaN [54,55]. The main hybridization attributes to N-*p*, Ga-*p* and Ga-*s* appears in the subband near VBM. Besides *s* and *p* orbitals, the states nears the VBM are also contributed by Ga-*3d* orbital (origin solid lines in Fig. 6(a)). That is, Ga-*3d* mediates *s-p* hybridization. During this process, due to the mediation of Ga-*3d* orbital, the contribution to Ga-N covalent bond from Ga-*p* orbital is suppressed (purple solid lines), and the contribution from N-*p* orbital is elevated (green dotted lines). Hence, Ga-N bond in H-GaN would be strongly polarized.

The inhomogeneous distribution of charge density would induce disturbing Coulomb interaction during atom's thermal vibration, thus leading to low phonon lifetime. With strain increasing from 0% to 10%, the charge transfer between Ga and N atom decreases from 0.97 e^- to 0.91 e^- (Fig. 6(b)). The less charge transfer means the Ga-N bond is less polarized. The decreased charge transfer can also be revealed from the shrinking of isosurface of deformation charge density in Fig. 6(c). As can be seen from above, the charge density distribution will be more homogeneous with increasing tensile strain, and the additional Coulomb forces during atom vibration will be suppressed, and the phonon lifetime will increase accordingly.

However, the atom vibration anharmonicity is not only influenced by the perturbation to bond by the electrostatic forces, but also by the strength of bond itself. To show the change of Ga-N pair strength, integrated crystal orbital Hamilton population (ICOHP) is calculated in Fig. 6(d). By analyzing the bonding and antibonding states under Fermi level, ICOHP quantifies the bonding strength between atom pairs [56]. A lower ICOHP value implies the stronger covalent bond. ICOHP of H-GaN increases from −4.4 to −3.8 with strain increases from 0% to 10%, indicating the weakened Ga-N covalent bond. In addition, the weakened bond strength is consistent with the increase of Ga-N bond length as shown in Fig. 6(b). The weakened bond strength makes the atom to vibrate at a larger amplitude, resulting in strong vibration anharmonicity. And the increased anharmonicity will suppress the phonon lifetime. Moreover, the weakened bond strength will lead to lower Young's modulus and group velocity as discussed before.

For phonon lifetime, it can be found that there are two competing factors. One is the decrease of Ga-N bond polarization, and the other is the weakening of covalent bond strength. When the tensile strain is small, the polarization factor is dominant, while the influence of increasing thermal vibration displacement cannot be ignored under large strain. As a result of the competition between the two factors, the phonon lifetime of H-GaN increases during the strain of 0% to 6%, and decreases with strain increasing from 6% to 10%. Therefore, the fundamental understanding of phonon lifetime variation is achieved from the perspective of changes in electronic structure.

3.5. Strain-dependent size effect

When the length scale of system is lower than the mean free path of phonons, the phonon–phonon scattering event is largely inhibited, which is also called as "ballistic transport" [57]. And the thermal conductivity at nanoscale will depend on the length, that is, the size effect. Size reduction is an effective strategy to regulate thermal conductivity without changing the electrical properties. The normalized cumulative lattice thermal conductivity under different strain level is shown in Fig. 7. The phonon mean free path (MFP) characterizes how phonons with different MFPs contribute to total thermal conductivity. Thermal conductivity under strain of 6% gives the largest value in the infinite case, as expected, a significant amount is contributed by phonons with relatively larger MFP. To characterize the size effect more quantitatively, we fit the data to a single parametric function [58]

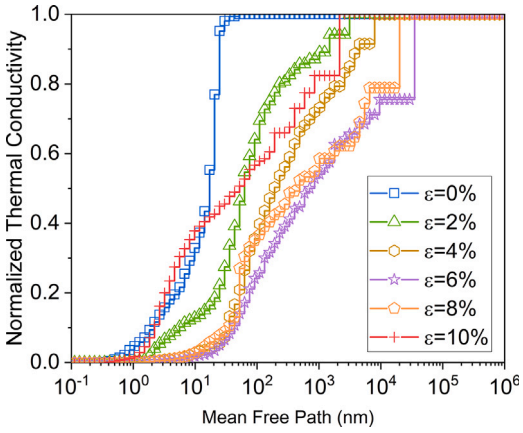

Fig. 7. The normalized accumulative thermal conductivity with respect to phonon mean free path.

$$k_l(l_{MFP}) = \frac{k_{max}}{1 + \frac{l_r}{l_{MFP}}} \tag{5}$$

where k_{max}, l_r and l_{MFP} represent for maximal lattice thermal conductivity, representative MFP (rMFP) and MFP, respectively. The fitted values of characteristic MFP of H-GaN are shown in Table 1. rMFP is helpful for the study of the ballistic phonon transport in nanostructuring. rMFP of H-GaN increases from 11.0 nm to 813.9 nm with strain increasing from 0% to 6%, then decreases to 46.5 nm at the strain of 10%. The relatively small rMFP at strain of 0% indicates the difficulty to modulate thermal transport properties by nanostructuring. As tensile strain increases, the tunability of nanostructure size on H-GaN shows an up-then-down trend. This indicates that strain combining nanostructure engineering could regulate the thermal transport properties of H-GaN well due to size effect.

4. Conclusions

In summary, by first-principle and phonon BTE calculations, we have performed a detailed study on strain-dependent thermal transport properties of hydrogenated 2D GaN. The thermal conductivity of H-GaN rises first and then descends with the increase of strain. Our study shows that the phonon lifetime governs the trend of thermal conductivity. All three acoustic modes' lifetime in H-GaN show up-then-down behaviors, which lead to a same trend of thermal conductivity. And the underlying mechanism for the response of modes' lifetime to strain can be well understood by atom vibration anharmonicity. Ga *3d* orbital mediates the hydrogenation between Ga-N pair, which leads to highly polarized covalent bond. As the strain increases, there is a competition between the effects of decrease of polarity and weakening of bond strength, and the two factors together lead to a up-then-down trend of phonon lifetime. By MFP analysis, it is found that tensile strain also induces an up-then-down size effect. Our study provides a comprehensive understanding for the strain-dependent thermal transport properties in hydrogenated 2D GaN and it will enrich the study of 2D GaN and provide prospective guidance for the experiment.

CRediT authorship contribution statement

Guoqing Sun: Writing – original draft, Formal analysis, Data curation, Conceptualization. **Yanhua Cheng:** Methodology, Formal analysis. **Jinlong Ma:** Investigation, Formal analysis. **Dongwei Xu:** Writing – review & editing, Supervision, Funding acquisition. **Xiaobing Luo:** Writing – review & editing, Visualization.

Declaration of competing interest

The authors declare that they have no known competing financial interests or personal relationships that could have appeared to influence the work reported in this paper.

Data availability

Data will be made available on request.

Acknowledgments

D. X. acknowledges the support from the National Natural Science Foundation of China, China (No. 51806072). And this work is done at zhonghe II supercomputer in the Jiangsu Century-horizon Information Technology Co,Ltd at Nanjing.

Appendix A. Supplementary data

Supplementary material related to this article can be found online at https://doi.org/10.1016/j.vacuum.2023.111808.The convergence test in calculating the thermal conductivity and the structure stability test during AIMD simulation.

References

[1] Y.X. Chen, J.X. Liu, K.L. Liu, J.J. Si, Y.R. Ding, L.Y. Li, T.R. Lv, J.P. Liu, L. Fu, GaN in different dimensionalities: Properties, synthesis, and applications, Mater. Sci. Eng. R 138 (2019) 60–84.
[2] J.L. Ma, W. Li, X.B. Luo, Intrinsic thermal conductivities and size effect of alloys of wurtzite AlN, GaN, and InN from first-principles, J. Appl. Phys. 119 (12) (2016) 125702.
[3] S. Nakamura, M.R. Krames, History of gallium–nitride-based light-emitting diodes for illumination, Proc. IEEE 101 (10) (2013) 2211–2220.
[4] L. Hu, X.Y. Ren, J.P. Liu, A.Q. Tian, L.R. Jiang, S.Y. Huang, W. Zhou, L.Q. Zhang, H. Yang, High-power hybrid GaN-based green laser diodes with ITO cladding layer, Photon. Res. 8 (3) (2020) 279–285.
[5] Z.Z. Qin, G.Z. Qin, X. Zuo, Z.H. Xiong, M. Hu, Orbitally driven low thermal conductivity of monolayer gallium nitride (GaN) with planar honeycomb structure: a comparative study, Nanoscale 9 (12) (2017) 4295–4309.
[6] X.R. Cai, Y.M. Ma, J.L. Ma, D.W. Xu, X.B. Luo, Structure and electronic bandgap tunability of m-plane GaN multilayers, Phys. Chem. Chem. Phys. 23 (2021) 5431–5437.
[7] N. Sanders, D. Bayerl, G. Shi, K.A. Mengle, E. Kioupakis, Electronic and optical properties of two-dimensional GaN from first-principles, Nano Lett. 17 (12) (2017) 7345–7349.
[8] X.R. Cai, G.Q. Sun, Y.X. Xu, J.L. Ma, D.W. Xu, Effect of hydrogenation on the thermal conductivity of 2D gallium nitride, Phys. Chem. Chem. Phys. 23 (39) (2021) 22423–22429.
[9] Z.Y. Al Balushi, K. Wang, R.K. Ghosh, R.A. Vilá, S.M. Eichfeld, J.D. Caldwell, X. Qin, Y.-C. Lin, P.A. DeSario, G. Stone, et al., Two-dimensional gallium nitride realized via graphene encapsulation, Nature Mater. 15 (11) (2016) 1166–1171.
[10] D. Hoat, S. Amirian, H. Alborznia, A. Laref, A. Reshak, M. Naseri, Strain effect on the electronic and optical properties of 2D tetrahexcarbon: A DFT-based study, Indian J. Phys. 95 (11) (2021) 2365–2373.
[11] H.B. Shu, X.H. Niu, X.J. Ding, Y. Wang, Effects of strain and surface modification on stability, electronic and optical properties of GaN monolayer, Appl. Surf. Sci. 479 (2019) 475–481.
[12] D. Hoat, M. Naseri, T.V. Vu, H.L. Luong, N.N. Hieu, R. Ponce-Pérez, J. Rivas-Silva, G.H. Cocoletzi, Biaxial strain and external electric field effects on the electronic structure of hydrogenated GaN monolayer, Superlattices Microstruct. 136 (2019) 106270.
[13] K. Du, Z.H. Xiong, L. Ao, L.L. Chen, Tuning the electronic and optical properties of two-dimensional gallium nitride by chemical functionalization, Vacuum 185 (2021) 110008.
[14] X.R. Cai, Y.Y. Ren, M.H. Wu, D.W. Xu, X.B. Luo, Strain-induced phase transition and giant piezoelectricity in monolayer tellurene, Nanoscale 12 (2020) 167–172.
[15] Y. Chen, J. Washburn, Structural transition in large-lattice-mismatch heteroepitaxy, Phys. Rev. Lett. 77 (1996) 4046–4049.
[16] Y. Chen, K. Liu, J. Liu, T. Lv, B. Wei, T. Zhang, M. Zeng, Z. Wang, L. Fu, Growth of 2D GaN single crystals on liquid metals, J. Am. Chem. Soc. 140 (48) (2018) 16392–16395.
[17] C.D. Mendoza, I.J. Califrer, F.L. Freire Jr., Strain in twisted bilayer graphene grown by chemical vapour deposition on Ni surfaces, Appl. Surf. Sci. 544 (2021) 148884.
[18] J. Du, H. Yu, B. Liu, M. Hong, Q. Liao, Z. Zhang, Y. Zhang, Strain engineering in 2D material-based flexible optoelectronics, Small Methods 5 (1) (2021) 2000919.
[19] M.J. Abdulameer, S.S. Abed Al-Abbas, H.R. Jappor, Tuning optical and electronic properties of 2D ZnI2/CdS heterostructure by biaxial strains for optical nanodevices: A first-principles study, J. Appl. Phys. 129 (22) (2021) 225104.
[20] Y. Mao, R. Wu, D. Ding, F. He, Tunable optoelectronic properties of two-dimensional PbSe by strain: First-principles study, Comput. Mater. Sci. 202 (2022) 110957.
[21] X. Xu, T. Liang, D. Kong, B. Wang, L. Zhi, Strain engineering of two-dimensional materials for advanced electrocatalysts, Mater. Today Nano 14 (2021) 100111.
[22] J. Quereda, P. San-Jose, V. Parente, L. Vaquero-Garzon, A.J. Molina-Mendoza, N. Agraït, G. Rubio-Bollinger, F. Guinea, R. Roldán, A. Castellanos-Gomez, Strong modulation of optical properties in black phosphorus through strain-engineered rippling, Nano Lett. 16 (5) (2016) 2931–2937.
[23] H.H. Peérez Garza, E.W. Kievit, G.F. Schneider, U. Staufer, Controlled, reversible, and nondestructive generation of uniaxial extreme strains (>10%) in graphene, Nano Lett. 14 (7) (2014) 4107–4113.
[24] S. Manzeli, A. Allain, A. Ghadimi, A. Kis, Piezoresistivity and strain-induced band gap tuning in atomically thin MoS2, Nano Lett. 15 (8) (2015) 5330–5335.
[25] A. Azcatl, X. Qin, A. Prakash, C. Zhang, L. Cheng, Q. Wang, N. Lu, M.J. Kim, J. Kim, K. Cho, et al., Covalent nitrogen doping and compressive strain in MoS2 by remote N2 plasma exposure, Nano Lett. 16 (9) (2016) 5437–5443.
[26] G.Z. Qin, Z.Z. Qin, H.M. Wang, M. Hu, Lone-pair electrons induced anomalous enhancement of thermal transport in strained planar two-dimensional materials, Nano Energy 50 (2018) 425–430.
[27] S.-D. Guo, J. Dong, Biaxial tensile strain tuned up-and-down behavior on lattice thermal conductivity in β-AsP monolayer, J. Phys. D: Appl. Phys. 51 (26) (2018) 265307.
[28] H. Xie, T. Ou Yang, É. Germaneau, G.Z. Qin, M. Hu, H. Bao, Large tunability of lattice thermal conductivity of monolayer silicene via mechanical strain, Phys. Rev. B 93 (2016) 075404.
[29] A.X. Zhang, J.T. Liu, S.D. Guo, H.C. Li, Strain effects on phonon transport in antimonene investigated using a first-principles study, Phys. Chem. Chem. Phys. 19 (2017) 14520–14526.
[30] M.H. Rahman, E.H. Chowdhury, D.A. Redwan, S. Hong, Computational characterization of thermal and mechanical properties of single and bilayer germanene nanoribbon, Comput. Mater. Sci. 190 (2021) 110272.
[31] K.P. Yuan, X.L. Zhang, L. Li, D.W. Tang, Effects of tensile strain and finite size on thermal conductivity in monolayer WSe2, Phys. Chem. Chem. Phys. 21 (2019) 468–477.
[32] B. Mortazavi, M.-Q. Le, T. Rabczuk, L.F.C. Pereira, Anomalous strain effect on the thermal conductivity of borophene: A reactive molecular dynamics study, Physica E 93 (2017) 202–207.
[33] K. Dabsamut, T. Thanasarnsurapong, T. Maluangnont, J. T-Thienprasert, S. Jungthawan, A. Boonchun, Strain engineering and thermal conductivity of a penta-BCN monolayer: a computational study, J. Phys. D: Appl. Phys. 54 (35) (2021) 355301.
[34] Y. Gao, W.Z. Yang, B.x. Xu, Unusual thermal conductivity behavior of serpentine graphene nanoribbons under tensile strain, Carbon 96 (2016) 513–521.
[35] H.K. Liu, G.Z. Qin, Y. Lin, M. Hu, Disparate strain dependent thermal conductivity of two-dimensional penta-structures, Nano Lett. 16 (6) (2016) 3831–3842.
[36] J.P. Perdew, K. Burke, M. Ernzerhof, Generalized gradient approximation made simple, Phys. Rev. Lett. 77 (1996) 3865–3868.
[37] G. Kresse, J. Furthmüller, Efficient iterative schemes for ab initio total-energy calculations using a plane-wave basis set, Phys. Rev. B 54 (1996) 11169–11186.
[38] G. Kresse, J. Furthmüller, Efficiency of ab-initio total energy calculations for metals and semiconductors using a plane-wave basis set, Comput. Mater. Sci. 6 (1) (1996) 15–50.
[39] W. Li, J. Carrete, N.A. Katcho, N. Mingo, ShengBTE: A solver of the Boltzmann transport equation for phonons, Comput. Phys. Comm. 185 (6) (2014) 1747–1758.
[40] X. Yang, D. Han, H. Fan, M. Wang, M. Du, X. Wang, First-principles calculations of phonon behaviors in graphether: A comparative study with graphene, Phys. Chem. Chem. Phys. 23 (1) (2021) 123–130.
[41] Y. Cheng, J. Ma, Y. Xu, G. Sun, X. Ruan, X. Luo, Evolution of in-plane heat transport in tellurium from 2D to 3D, Mater. Today Phys. (2022) 100776.
[42] A. Togo, F. Oba, I. Tanaka, First-principles calculations of the ferroelastic transition between rutile-type and $CaCl_2$-type SiO_2 at high pressures, Phys. Rev. B 78 (2008) 134106.

[43] W. Li, L. Lindsay, D.A. Broido, D.A. Stewart, N. Mingo, Thermal conductivity of bulk and nanowire $Mg_2Si_xSn_{1-x}$ alloys from first principles, Phys. Rev. B 86 (2012) 174307.
[44] X. Wu, V. Varshney, J. Lee, Y. Pang, A.K. Roy, T. Luo, How to characterize thermal transport capability of 2D materials fairly?–Sheet thermal conductance and the choice of thickness, Chem. Phys. Lett. 669 (2017) 233–237.
[45] M. Kiyashko, P. Grinchuk, T. Kuznetsova, A. Kren, H. Abuhimd, Determination of elastic modulus of SiC-based composite ceramics, Tech. Phys. Lett. 47 (2) (2021) 150–153.
[46] A. Taheri, S. Pisana, C.V. Singh, Importance of quadratic dispersion in acoustic flexural phonons for thermal transport of two-dimensional materials, Phys. Rev. B 103 (23) (2021) 235426.
[47] F.Q. Wang, J. Yu, Q. Wang, Y. Kawazoe, P. Jena, Lattice thermal conductivity of penta-graphene, Carbon 105 (2016) 424–429.
[48] L.-F. Huang, P.-L. Gong, Z. Zeng, Phonon properties, thermal expansion, and thermomechanics of silicene and germanene, Phys. Rev. B 91 (20) (2015) 205433.
[49] Y. Dou, J. Li, Y. Xie, X. Wu, L. Hu, F. Liu, W. Ao, Y. Liu, C. Zhang, Lone-pair engineering: Achieving ultralow lattice thermal conductivity and enhanced thermoelectric performance in Al-doped GeTe-based alloys, Mater. Today Phys. 20 (2021) 100497.
[50] A. Lou, Q.-B. Liu, H.-H. Fu, Enhanced thermoelectric performance by lone-pair electrons and bond anharmonicity in the two-dimensional Ge 2 Y 2 family of materials with Y=N, P, As, or Sb, Phys. Rev. B 105 (7) (2022) 075431.
[51] Z. Lin, G. Wang, C. Le, H. Zhao, N. Liu, J. Hu, L. Guo, X. Chen, Thermal conductivities in NaSnAs, NaSnP, and NaS n 2 A s 2: Effect of double lone-pair electrons, Phys. Rev. B 95 (16) (2017) 165201.
[52] M.K. Jana, K. Pal, U.V. Waghmare, K. Biswas, The origin of ultralow thermal conductivity in InTe: Lone-pair-induced anharmonic rattling, Angew. Chem. 128 (27) (2016) 7923–7927.
[53] G. Qin, Z. Qin, H. Wang, M. Hu, Lone-pair electrons induced anomalous enhancement of thermal transport in strained planar two-dimensional materials, Nano Energy 50 (2018) 425–430.
[54] M. Magnuson, M. Mattesini, C. Höglund, J. Birch, L. Hultman, Electronic structure of GaN and Ga investigated by soft X-ray spectroscopy and first-principles methods, Phys. Rev. B 81 (8) (2010) 085125.
[55] M. Ptasinska, J. Sołtys, J. Piechota, S. Krukowski, Electronic properties on GaN (0001) surface–ab initio investigation, Vacuum 99 (2014) 166–174.
[56] S. Steinberg, R. Dronskowski, The crystal orbital hamilton population (COHP) method as a tool to visualize and analyze chemical bonding in intermetallic compounds, Crystals 8 (5) (2018) 225.
[57] Y. Hu, L. Zeng, A.J. Minnich, M.S. Dresselhaus, G. Chen, Spectral mapping of thermal conductivity through nanoscale ballistic transport, Nature Nanotechnol. 10 (8) (2015) 701–706.
[58] G. Qin, Z. Qin, W.-Z. Fang, L.-C. Zhang, S.-Y. Yue, Q.-B. Yan, M. Hu, G. Su, Diverse anisotropy of phonon transport in two-dimensional group IV–VI compounds: A comparative study, Nanoscale 8 (21) (2016) 11306–11319.